Available online at www.sciencedirect.com
SCIENCE DIRECT®
Journal of Power Sources 119–121 (2003) 743–748
JOURNAL OF POWER SOURCES
www.elsevier.com/locate/jpowsour

Spectroscopic studies of the structural transitions in positive electrodes for lithium batteries

C.M. Julien[a,*], M. Massot[b]

[a]Laboratoire des Milieux Désordonnés et Hétérogènes, UMR 7603, Université Pierre et Marie Curie, 4 place Jussieu, Case 86, 75252 Paris Cedex 05, France
[b]Laboratoire de Physique des Milieux Condensés, UMR 7602, Université Pierre et Marie Curie, 4 place Jussieu, Case 77, 75252 Paris Cedex 05, France

Abstract

We present the vibrational features of MnO_2, $Li_{0.33}MnO_2$, Li_xCoO_2 and $Li_xMn_2O_4$ used as positive electrode materials in lithium batteries. Raman and FTIR spectroscopies yield a reliable description of lattice when either crystalline disorder or phase transition due to Li insertion is expected. The local arrangement in the γ-MnO_2 structure is investigated as a function of the pyrolusite intergrowth rate. The phase evolution in Li_xCoO_2 and $Li_xMn_2O_4$ is studied as a function of the degree of deintercalation.

Keywords: FTIR spectroscopy; Transition-metal oxides; Manganese dioxides (MDOs)

1. Introduction

Stimulated investigations of transition-metal oxides, which are currently used as positive electrodes in rechargeable lithium batteries, have been directed toward high electrochemical efficiency [1–3]. Among these materials, we consider the following systems: manganese dioxides (MDOs), 2D $LiCoO_2$ oxides with the α-$NaFeO_2$-type structure, and 3D spinel $LiMn_2O_4$. Since their electrochemical features depend on their crystal nature, size and shape, various kinds of preparation methods have been developed to improve their characteristics, such as rechargeability and the capacity retention upon cycling. The current debate consists in the investigation of the local structure of these compounds because of the difficulty encountered in using powder X-ray and neutron diffraction for an unambiguous structural determination.

Among the local probes, Raman scattering (RS) and Fourier transform infrared (FTIR) spectroscopy are techniques sensitive to the short-range environment of oxygen coordination around the cations [4]. As a first approximation, spectra consist of a superposition of the components of all local entities present in the same material in contrast to diffraction data which give a weighted average of similar interplanar spacing. As a general rule, the frequencies and relative intensities of the bands are sensitive to coordination geometry and oxidation states.

In this paper, we present the vibrational features of γ-MnO_2, $Li_{0.33}MnO_2$, Li_xCoO_2 and $Li_xMn_2O_4$. We investigate the local structure in γ-MnO_2 as a function of the pyrolusite intergrowth rate. We report structural features of $Li_{0.33}MnO_2$ and those of Li_xCoO_2 and $Li_xMn_2O_4$ as a function of the degree of deintercalation. Experimental procedures are those described elsewhere [5].

2. Vibrational features of MnO_2

The XRD patterns of γ-MnO_2 powders are of rather poor quality and consist at best of a small number of sharp and broad lines on top of a diffuse background. The structure of γ-MnO_2 can be seen as an intergrowth (Pr value) of pyrolusite (β-MnO_2) blocks within a ramsdellite (R-MnO_2) matrix. The crystal chemistry led De Wolff to propose a structural model of γ-MnO_2 based on the observation that rutile and ramsdellite structures have similar arrangements along their *a* and *c* axes and differ only by the width of the infinite strings of MnO_6 octahedra along the *b* axis [6]. The procedure established by Pannetier uses the position of the (1 1 0) Bragg line and the difference in degrees 2θ between the (2 1 1) and (2 4 0) reflections to determine Pr [7].

A careful examination of the spectroscopic results published earlier by workers and of those that are more recently

* Corresponding author. Tel.: +33-144-274561; fax: +33-144-273854.
E-mail address: cjul@ccr.jussieu.fr (C.M. Julien).

0378-7753/03/$ – see front matter © 2003 Published by Elsevier Science B.V.
doi:10.1016/S0378-7753(03)00214-3

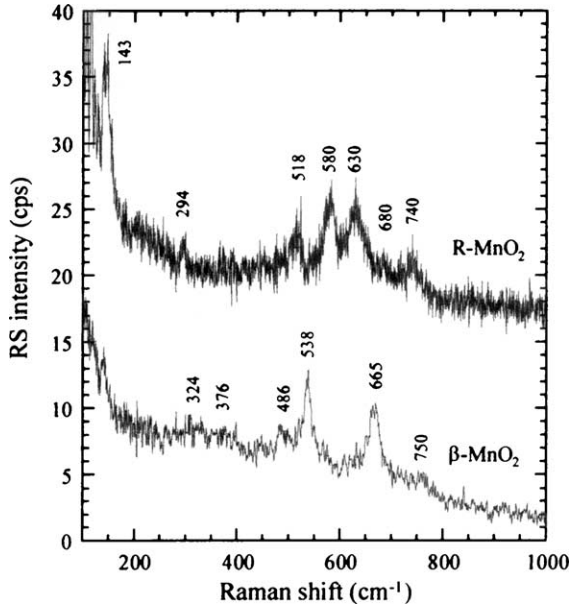

Fig. 1. Raman spectra of ramsdellite (R-MnO_2) and pyrolusite (β-MnO_2).

appeared shows discordance regarding the Raman spectra of MnO_2 due to the general peculiarity of low Raman activity of vibrational features in MDOs [8–11]. All measurements are concerned with the mid-infrared region 400–4000 cm^{-1} but they did not pay attention to the far-infrared region 100–800 cm^{-1} where IR is sensitive to octahedra polymerisation, which provides a means to measure the concentration of pyrolusite microdomains in γ-MnO_2.

Figs. 1 and 2 shows the RS and FTIR spectra, respectively, of the end members of the nsutite family, β-MnO_2 and R-MnO_2. Raman features of MnO_2 are very weak even for well-crystallised compounds. The RS spectrum of β-MnO_2 has relatively sharp peaks indicative of a well-developed rutile-type structure with an interstitial space consisting of narrow one-dimensional $T_{1,1}$ channels. The main contributions are attributed to the stretching mode of the MnO_6 octahedra. The corresponding anti-symmetric stretching modes are recorded in the FTIR spectrum at 517 and 621 cm^{-1}. RS peaks at lower frequencies are attributed to the deformation modes of the metal-oxygen chain of Mn–O–Mn in the MnO_2 octahedral lattice. The RS spectrum of R–MnO_2 displays three main contributions which are indicative of a well-developed orthorhombic structure with an interstitial space consisting of $T_{1,2}$ channels.

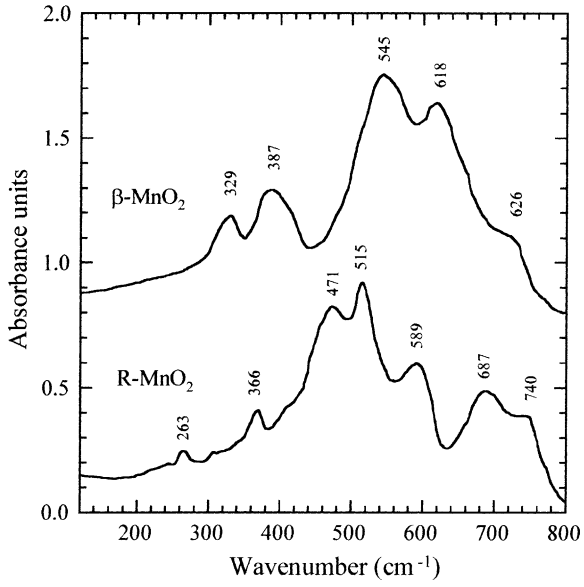

Fig. 2. FTIR absorption spectra of ramsdellite (R-MnO_2) and pyrolusite (β-MnO_2).

The spectral identification of the polymerisation by edge-sharing of the MnO_6 octahedra in MDOs was obtained from Raman data. Fig. 3 presents the frequency position of the major Raman-active modes as a function of the average MnO_6 octahedral polymerisation in several MDOs structures. A trend is also observed showing a general decrease in band wavenumber with increasing octahedral polymerisation. The two sets of stretching modes, noted ν_1 and ν_2, allow a direct comparison between the Raman patterns of manganese oxides. Starting from pyrolusite with two shared edges per MnO_6 octahedron, one reaches the point for manganosite (MnO having the NaCl structure) with eight shared edges per MnO_6 octahedron that gave the lowest wavenumber $\nu_1 = 531$ cm^{-1}. To apply this correlation, the position of the low-energy Raman band of the birnessite $MnO_{1.86}{\cdot}0.6H_2O$ supports its proposed layered structure, which places it at 4.8 shared edges per octahedron.

RS spectra of γ-MnO_2 have been recorded for various Pr-values. Knowing that, as a first approximation, spectra consist of a superposition of the components of all local entities, a careful examination show further behaviour. RS features exhibit variations in band position and intensity which cannot be reproduced by addition of various proportions of pyrolusite and ramsdellite spectra [12]. Fig. 4 displays the RS

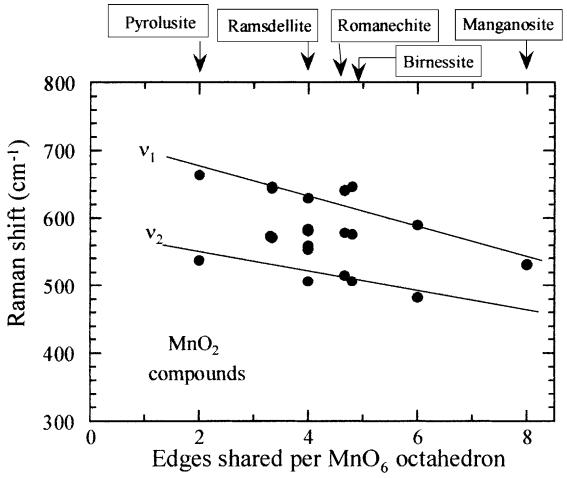

Fig. 3. Frequency position of the Raman-active modes as a function of the average MnO_6 octahedral polymerisation in various MDOs. Dots represent the predominant Raman bands.

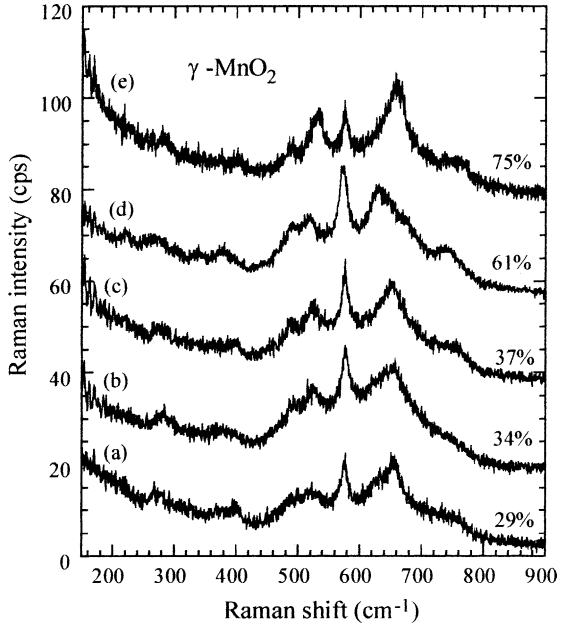

Fig. 4. RS spectra of γ-MnO_2 with various Pr values. Sample numbers are (a) γ-MnO_2 with Pr = 29%, (b) γ-MnO_2 with Pr = 34% (Hoechst), (c) γ-MnO_2 with Pr = 37% (EMD activated), (d) γ-MnO_2 EMD with Pr = 61%, (e) γ-MnO_2 (Puratronic, Alpha-Ventron) with Pr = 75%.

spectra of five γ-MnO_2 compounds electrochemically synthesised with $29 \leq Pr \leq 75\%$. Except for a sample with Pr = 61%, all the bands are shifted toward the high-frequency side as Pr increases; this is due to the increasing concentration of pyrolusite microdomains in the γ-MnO_2 matrix. Therefore, the bands in the range 500–700 cm^{-1} are considered as the characteristic features of γ-MnO_2. A close examination of this spectral region allows to consider the three main bands of R–MnO_2, noted ν_2, ν_3, and ν_4. As the amount of pyrolusite defect increases in the ramsdellite network, we observe a frequency shift of the bands ν_2 and ν_4 toward those of β-MnO_2 phase (at higher wavenumber) while ν_3 remains almost at the same position. The pyrolusite-like peak at 630 cm^{-1} appears as a shoulder in the γ-MnO_2 phase with Pr = 61%, while the band at 654 cm^{-1} is located in between ν_2 of R-MnO_2 (630 cm^{-1}) and ν_2 of β-MnO_2 (665 cm^{-1}).

Fig. 5 presents the variation of the Raman band frequencies as a function of the structural parameter Pr in γ-MnO_2 showing an accurate elucidation of the quantitative determination of the structural disorder present in γ-MnO_2. A linear relationship exists between the Raman frequency of the three main bands and Pr. Because MDOs are constituted of condensed polyhedra interlinked by either edges or corners (such as in spinel structures), we must consider the possibility of vibrational interactions between identical octahedra. Considering the local structure of γ-MnO_2 compounds, the MnO_6 octahedra are edge sharing groups, much more important vibrational interactions are expected in the direction of the O–Mn–O–Mn–O chains. According to the classical structural model for the nsutite-type compounds, defects expand in the directions perpendicular to the chains

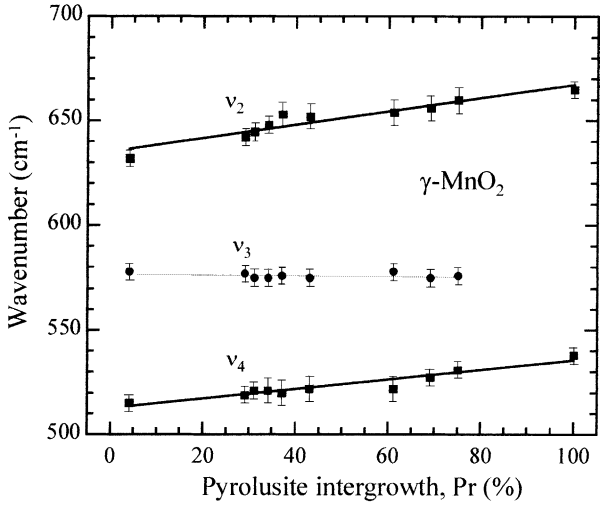

Fig. 5. Variation of Raman frequencies as a function of the structural parameter Pr in γ-MnO_2.

and consequently influence the lattice vibrations of condensed octahedra with respect to that of isolated species.

3. Vibrational features of $Li_{0.33}MnO_2$

Fig. 6a–b shows the vibrational spectra of lithiated $Li_{0.33}MnO_2$. The crystal structure of $Li_{0.33}MnO_2$ examined

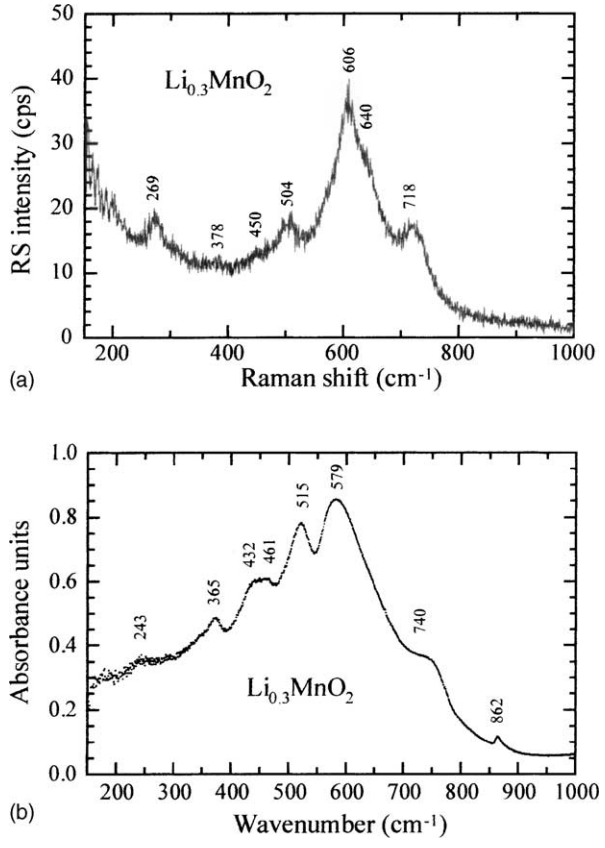

Fig. 6. Raman and FTIR spectra of $Li_{0.3}MnO_2$.

by XRD corresponds to a new MnO_2 with an ordered alternation of (1×2) and (1×1) channels of the γ-MnO_2 phase. RS and FTIR as local probes show that lithium ions are located in octahedral sites in the (1×2) channels. Significant changes are seen in the MnO_6 octahedral arrangement from sample to sample by examining the spectra in a high-frequency region compared with their parents that are pyrolusite and ramsdellite. The IR peak at 579 cm^{-1} corresponds to the anti-symmetric stretching mode of the MnO_6 octahedra. As this peak appears at 618 cm^{-1} in β-MnO_2, we assume that the lithiation proceeds with a frequency shift of the MoO_6 stretch due to the change in the average Mn valency and the modification in the chemical bonding of the MoO_6 octahedra in the $Li_{0.3}MnO_2$ lattice. The comparison of spectra of either R-MnO_2 or β-MnO_2 with $Li_{0.3}MnO_2$ in the far-infrared region (below 300 cm^{-1}) leads that the appearance of the peak at 243 cm^{-1} is the consequence of the lithiation.

4. Lattice dynamics of Li_xCoO_2

$LiCoO_2$ has been proposed as a cathode for a lithium battery by Mizushima et al. [13] and currently it is being used in commercial rechargeable Li-ion batteries. Fig. 7 displays the FTIR absorption spectra of Li_xCoO_2 cathode-active materials as a function of x(Li). As predicted from the factor group analysis, one observes four distinct IR bands at 269, 420, 539, and 602 cm^{-1} along with a shoulder at 646 cm^{-1}. To get a better understanding, we consider the $LiCoO_2$ structure which consists of compressed CoO_6 and elongated LiO_6 octahedra that yields distinct vibrations in two different regions, i.e. at 400–650 cm^{-1} there are bands due to

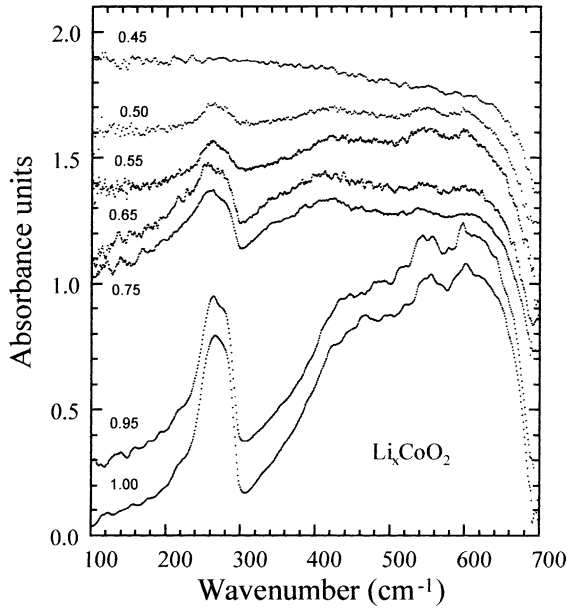

Fig. 7. FTIR absorption spectra of Li_xCoO_2 as a function of x(Li) in the range $0.4 \leq x \leq 1.0$.

CoO_6 vibrations (Co–O stretching and O–Co–O bending), while the LiO_6 stretching mode appears at 269 cm^{-1} [14].

Upon lithium de-intercalation changes are as follows: (a) a decrease of the oscillator strength and a broadening of all the IR-bands can be associated to a disorder induced by the departure of Li-ions located between two CoO_2 blocks. The broadening of the low-frequency band can be also attributed to the random distribution of the Li-ions remaining in the host matrix; (b) no frequency change is observed for the high-wavenumber bands which are assigned to the CoO_6 vibrations. Thus, as expected, we can conclude that the CoO_2 layers are not affected significantly by the lithium de-intercalation process; (c) a significant shift of the low-frequency band is recorded. This band shifts toward the low-energy side from 269 to 258 cm^{-1} in $Li_{0.5}CoO_2$. The frequency shift corresponds to the increase in the interlayer spacing due to an increase of the repulsive interactions between two adjacent negatively charged CoO_2 layers upon de-lithiation. Thus, the interlayer force constant is reduced by about 8%. (d) The increase of the far-infrared absorption of the $Li_{0.4}CoO_2$ sample is attributed to the Drude edge due to the change in the electrical conductivity of the material. This suggests the existence of collective delocalized electrons. These results agree well with the p-type semi-conducting character of $LiCoO_2$ (band gap $E_g = 2.7$ eV) while Li_xCoO_2 for $x \leq 0.75$ has a metal-like behaviour [15]. For every Li removed from the $LiCoO_2$ lattice, an electron hole is created within the valence band. For $x < 0.75$, we expect that there are sufficient holes to allow for a significant degree of screening, and in this regime, the hole states in the valence bands are likely to be delocalized, such that Li_xCoO_2 exhibits metallic electronic properties. This behaviour is clearly observed in the FTIR absorption spectra where absorption by holes is observed in the low-wavenumber region. The occurrence of delocalised holes contribute to the free energy of the electrode, influencing both the energetic and entropic terms [15]. This could be at the origin of the two-phase region observed in the potential curves of the Li//$LiCoO_2$ cells. From IR data, we remark that $LiCoO_2$ is less sensitive to lithium content due to the higher bond covalency in the CoO_2 slabs than $LiNiO_2$ does. Consequently, the strong bond covalency in $LiCoO_2$, with reduced Co–O bond distance, results in stabilisation of Co^{III} in a low-spin ground state, and reduces the electronic conductivity of the compound. By de-intercalating lithium into materials, the repulsion of the negatively charged CoO_2 layers increases and the Co^{4+}/Co^{3+} redox couple offers the possibility of electronic transfer. This cation oxidation results in an increase of the conductivity due to the decrease of the covalent character of the CoO_2 slabs.

5. Vibrational features of $Li_xMn_2O_4$

FTIR results by Richardson and Ross [16], and Julien et al. [17] showed evolution of the IR bands for cubic $Li_xMn_2O_4$,

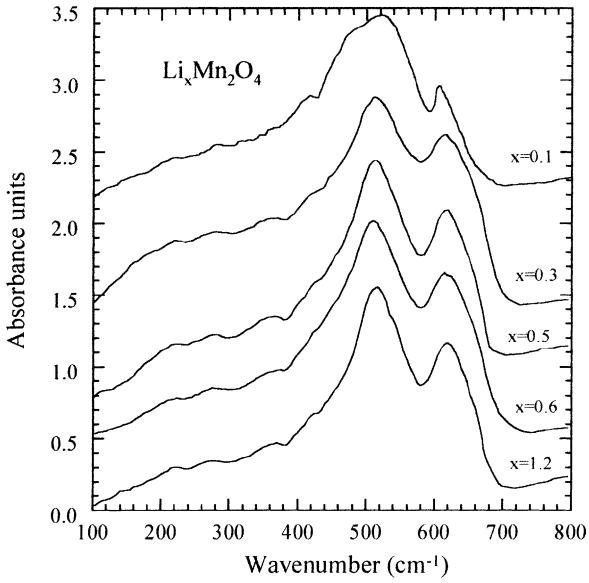

Fig. 8. FTIR spectra of the $Li_xMn_2O_4$ spinel as a function of x(Li) in the range $0.1 \leq x \leq 1.2$.

but could not clearly identify different cubic phases of $Li_xMn_2O_4$ when x varied from 0.1 to 1.0. Few works reported the far-IR spectra of $Li_xMn_2O_4$ spinel phases. Ammundsen et al. [18] have calculated the lattice dynamics of lithium manganese oxides using atomistic modelling methods. Recent in situ Raman studies on $Li_xMn_2O_4$ have been reported by Huang and Frech [19].

Fig. 8 shows the FTIR absorption spectra of the spinel $Li_xMn_2O_4$ as a function of the x(Li) in the range $0.1 \leq x \leq 1.2$. For $0.3 \leq x \leq 1.0$, IR spectra of delithiated phases have the same shape as the initial spinel $LiMn_2O_4$; they consist of a series of broad bands between 150 and 650 cm^{-1} which all correspond to modes with the F_{1u} symmetry (group factor analysis O_h^7). The FTIR spectrum of $LiMn_2O_4$ spinel is dominated by two strong absorption bands at ca. 619 and 513 cm^{-1}. Four weak bands are observed in the low-frequency region at ca. 225, 277, 367 and 420 cm^{-1}. The high-frequency bands located at ca. 619 and 513 cm^{-1} involve mainly displacement of oxide ions. They are attributed primarily to the asymmetric stretching modes of MnO_6 octahedra. It is obvious that such vibrations are rather more complex because an isolated MnO_6 octahedron does not exist in the spinel framework, but octahedra are connected with other MnO_6 octahedra and LiO_4 tetrahedra. Therefore, the low-frequency bands at ca. 225, 277 and 420 cm^{-1} can be primarily assigned to the deformation vibrations of the O–Mn–O groups, i.e. bending modes of MnO_6 octahedra. The weak IR-band at 367 cm^{-1} disappears for the delithiated $Li_{0.1}Mn_2O_4$ phase whereas the two other low-frequency bands at 225 and 277 cm^{-1} remain almost at the same frequency. The mode that has its principal origins in vibrations of the Li lattice is the one which disappears on removal of lithium ions. It is an experimental fact that the IR absorption bands related to the stretching vibrations of LiO_4 tetrahedra are generally found in the 350–500 cm^{-1} region [20]. This is true, however, only in the absence of important vibrational interactions between LiO_4 tetrahedra and the other coordinated groups present in the structure. It was recognised that the atomic displacements contributing to the infrared spectra of spinel phases vary from compound to compound, depending on the masses, charges, and chemical properties of ions. The stretch of the LiO_4 has appeared out at 472 cm^{-1} in Li_3PO_4 whereas the frequency 435 cm^{-1} is pointed in the spinel $LiFeCr_4O_8$ [20]. It was also demonstrated that, in inorganic oxide glasses, the IR resonant frequencies of alkali metal cations in their equilibrium positions are as cation mass dependent bands [21] Due to important vibrational interactions between LiO_4 tetrahedra and MnO_6 groups, this leads to the frequency at ca. 367 cm^{-1} for oscillation of the Li^+ ion against O^{2-} near neighbours in $LiMn_2O_4$.

6. Conclusion

RS and FTIR spectroscopies have proven to be useful tools for the identification of the nsutite γ-MnO_2 phases. Because of their sensitiveness to short range order, Raman and FTIR give more reliable information than X-ray diffraction when applied to structural defects in γ-MnO_2. We have been able to show that elucidation of the quantitative determination of the structural disorder present in γ-MnO_2 is accurate by RS spectroscopy. The comparison of spectra of either R-MnO_2 or β-MnO_2 with $Li_{0.3}MnO_2$ in the far-infrared region (below 300 cm^{-1}) leads that the appearance of the peak at 243 cm^{-1} is the consequence of the lithiation.

Infrared studies of λ-$LiMn_2O_4$ and $LiCoO_2$ have shown that the spectral modifications during the deintercalation of Li ions from the host lattice reflect the phases and structural modifications in these compounds. The increase of the far-infrared absorption of the $Li_{0.4}CoO_2$ sample is attributed to the Drude edge due to the change in the electrical conductivity of the material. This suggests the existence of collective delocalized electrons. The local environment model for $Li_xMn_2O_4$ shows that the stretching mode of structural LiO_4 entities occurs in the intermediate frequency region at 367 cm^{-1}.

References

[1] J. Hunter, J. Solid State Chem. 39 (1981) 142.
[2] M.M. Thackeray, P. Johnson, L. de Piciotto, P.G. Bruce, J.B. Goodenough, Mater. Res. Bull. 19 (1984) 179.
[3] T. Ohzuku, M. Kitagawa, T. Hirai, J. Electrochem. Soc. 137 (1990) 769.
[4] C. Julien, Solid State Ion. 136–137 (2000) 877.
[5] C. Julien, NATO Sci. Ser. II-81 (2002) 235.
[6] P.M. De Wolff, Acta Crystallogr. 12 (1959) 341.
[7] Y. Chabre, J. Pannetier, Prog. Solid State Chem. 23 (1995) 1.
[8] B.R. Strohmeier, D.M. Hercules, J. Phys. Chem. 88 (1984) 4923.

[9] F. Kapteijn, A.D. van Langeveld, J.A. Moulijn, A. Andreini, M.A. Vuurman, A.M. Turek, J.M. Jehng, I.E. Washs, J. Catal. 150 (1994) 94.
[10] D. Gosztola, M.J. Weaver, J. Electranal. Chem. Interf. Electrochem. 271 (1989) 141.
[11] M.C. Bernard, A. Hugot-Le Goff, B.V. Thi, S. Cordoba de Torresi, J. Electrochem. Soc. 140 (1993) 3065.
[12] C. Julien, S. Rangan, M. Lemal, M. Massot, D. Guyomard, J. Raman Spectrosc. 33 (2002) 223.
[13] K. Mizushima, P.C. Jones, J.B. Goodenough, Mater. Res. Bull. 15 (1980) 783.
[14] C. Julien, Ionics 6 (2000) 30.
[15] A. Van der Ven, M.K. Aydinol, G. Ceder, Mater. Res. Soc. Symp. Proc. 496 (1998) 121.
[16] T.J. Richardson, P.N. Ross Jr., Mater. Res. Bull. 31 (1996) 935.
[17] C. Julien, A. Rougier, E. Haro-Poniatowski, G.A. Nazri, Mol. Cryst. Liq. Cryst. 311 (1998) 81.
[18] B. Ammundsen, G.R. Burns, M.S. Islam, H. Kanoh, J. Rozière, J. Phys. Chem. 103 (1999) 5175.
[19] W. Huang, R. Frech, J. Power Sources 81/82 (1999) 616.
[20] J. Preudhomme, P. Tarte, Spectrochim. Acta 27A (1971) 845.
[21] G.J. Exarhos, W.N. Risen, Solid State Commun. 11 (1972) 755.